Analytical and Bioanalytical Chemistry (2019) 411:7327–7336
https://doi.org/10.1007/s00216-019-02112-6

RESEARCH PAPER

Efficient AuPd@GO-based electrochemical nanoprobe for sensitive detection of histone acetylase activity and its inhibitor

Qiong Liu[1] · Linfei Yang[1] · Yuqi She[2] · Yufang Hu[3,4]

Received: 14 July 2019 / Revised: 19 August 2019 / Accepted: 30 August 2019 / Published online: 13 September 2019

Abstract

Histone acetylase (HAT p300), which has aroused great concern in fundamental research and clinical applications, serves as one class of significant tumor markers. In our work, a sensitive electrochemical immunoassay for testing HAT p300 based on both graphene-assisted supported AuPd nanomaterial (AuPd@GO composite) and a typical amperometric *i-t* technique with fast response is developed favorably. The AuPd@GO-based sensing mechanisms are distributed as follows: the HAT p300 derived acetylation reaction occurs at the customized peptide-immobilized electrode; the AuPd@GO composite acts as carrier to immobilize acetyl antibody, thus constructing a sandwich-type electrochemical immunosensor via an antigen and antibody interaction; importantly, a distinct electrochemical signal could be caught due to the AuPd@GO nanomaterial with a favorable electrocatalytic property to the commercialized 3,3,5′,5′-tetramethyl benzidine solution (TMB). Taking advantage of AuPd@GO composite, the established immunosensor displays a wide linear range from 1 pM to 1000 nM, and the detection limit is 0.5 pM ($S/N = 3$) for HAT p300. Next, the biosensor is also used to analyze the inhibitor of HAT p300 successfully, which is promising for promoting the development of electrochemical HAT-related biodetection and drug discovery.

Keywords Graphene-assisted supported AuPd nanomaterial · Electrochemical immunoassay · Histone acetylase · Inhibitor · Amperometric *i-t* curve

Introduction

Protein posttranslational modification is a crucial event in adjusting protein function and guaranteeing protein-protein interaction [1–4]. Acetylation of lysine residues within the eukaryotic cells, as an ample posttranslational modification, takes place frequently [5, 6]. Currently, abnormal acetylation comes under observation in malignant cells as well as activity alteration of histone acetyltransferase (HAT) [7, 8]. The analysis of HATs has important implications in early diagnosis, occurrence, and development of diseases, such as cancers (leukemia, breast, and colorectal) or human developmental disorders [9, 10]. Actually, it is crucial that identifying acetylation sites and binding partners is conductive to the exploration of acetylation-dependent signaling pathways [11]. Essentially, the problem presented is the recognition for acetylation sites when multiple acetylations occur [12]. The use of sensitive radiolabeled 14C- or 3H-acetyl CoA substrates enables the determination of the acetylation sites and the identification of the acetylated proteins within all kinds of cells [13–15]. Nay, specific acetylated lysine residues are probed by peptide substrate–based Edman degradation [16] or chemically synthesized peptide-triggered acetylation in vitro [17], but unluckily, these methods are both destructive and indirect. For another, mass spectrometry is a regular method for exploring acetylation within purified proteins isolated from cells

Electronic supplementary material The online version of this article (https://doi.org/10.1007/s00216-019-02112-6) contains supplementary material, which is available to authorized users.

✉ Yuqi She
syq0922@csu.edu.cn

✉ Yufang Hu
huyufang@nbu.edu.cn

[1] Clinical Laboratory of Hunan Provincial People's Hospital, The First Affiliated Hospital of Hunan Normal University, Changsha 410006, Hunan, China

[2] Blood Transfusion Department, Xiangya Hospital of Central South University, Changsha 410008, Hunan, China

[3] Faculty of Materials Science and Chemical Engineering, Ningbo University, Ningbo 315211, Zhejiang, China

[4] State Key Laboratory of Chemo/Biosensing and Chemometrics, College of Chemistry and Chemical Engineering, Hunan University, Changsha 410082, Hunan, China

[18]. However, multiple acetylations make it difficult to identify acetylation sites, and it is necessary to develop a sensitive and pointed strategy for investigating HAT activity, which is very promising for biochemical research and pharmaceutical development.

It is the electrochemical immunosensor that has attracted tremendous interest owing to its high sensitivity, fast response time, low cost, and simple pretreatment [19, 20]. Among them is enzyme-based electrochemical immunosensor, which has drawn high-level concern due to the catalytic amplification property–derived high sensitivity [21]. However, the choice and use of this enzyme are subjected to some drawbacks including poor stability, complex immobilization, and temperature- or pH-sensitive pattern [22, 23]. In this case, various types of nanomaterials have been employed recently in enzyme-free electrochemical immunosensor to overcome these shortcomings [24, 25]. As widely used nanomaterials, Au nanoparticles exhibit good biocompatibility, nice conductivity and stability, and especially favorable catalytic activity [26–28]. Particularly, incorporating Pd with Au (AuPd) wins intensive focus; this is because Au can promote the electron transfer of Pd [29–31]. But for all this, AuPd nanomaterials have tendency aggregation, thus generating the inactivation of the catalysts, which is caused by their high relative surface area and weak stabilization. In this context, graphene and its derivatives have emerged as supports to immobilize nanocatalysts to resolve this problem, thus improving catalytic performances [32–35]. This is mainly thanks to their high specific surface area, good electrical conductivity, outstanding electrochemical stability, and abundant functional groups [36, 37]. Therefore, developing a sensitive AuPd@GO-based method for HAT p300 detection is worthwhile, yet challenging undertaking.

Herein, we associate AuPd@GO composite and the HAT p300–triggered acetylation for the first time. This composite with both the favorable conductivity and high surface area is employed as not only a recognition probe but also a signal probe to construct a new and simple electrochemical immunosensor for the HAT p300 analysis. Furthermore, the as-prepared composite itself can respond to 3,3,5′,5′-tetramethyl benzidine solution (TMB) by amperometric *i-t* curve. The proposed immunosensor exhibits a wide linear range and a fine detection limit for HAT p300 with good stability and reproducibility. The increasing sensitivity of the constructed biosensor is attributed to the AuPd@GO composite, which not only merely accelerates efficiently the electron transfer rate but also improves availably the loading of acetyl antibody. Then, good results are also acquired from the analysis of the inhibitor of HAT p300. The proposed method offers a hopeful alternative for the HAT p300 analysis in practical samples, not only that, which is paving the way for novel next-generation point-of-care testing (POCT) [38].

Experimental section

Materials and apparatus

HAT (p300, > 95%, SDS-PAGE, solution in 50 mM Tris-HCl, pH 7.5, containing 100 mM sodium chloride, 0.2% NP-40, 50 mM imidazole, and 10% glycerol), protein kinase A (PKA), acetylcholinesterase (AChE), terminal deoxynucleotide transferase (TdT), alkaline phosphatase (ALP), palladium chloride ($PdCl_2$), $HAuCl_4{\cdot}3H_2O$, and acetyl coenzyme A (Ac-CoA) were purchased from Shanghai Sigma-Aldrich (China). C646 was acquired from Shanghai Selleck (China). The substrate peptide (sequence, RGKGGKGLGKGGAKAC) and 3,3,5′,5′-tetramethyl benzidine solution (monocomponent, Biotech Grade) (TMB) were obtained by Shanghai Sangon Biotechnology Co. Ltd. Acetyl-antibody (Ab_{Ac}) was bought from Beijing Biosynthesis Biotechnology Co. Ltd. The preparation of graphene oxide (GO) was custom-synthesized by using graphite powder (99.99995%, 325 mesh, Alfa Aesar) according to the reference [39]. All the other chemicals of analytical grade were not purified before use. All of the aqueous solutions were prepared with twice-distilled water which was from the Millipore Milli-Q system. The preparation of used buffers was depicted in the Electronic Supplementary Material (ESM).

Electrochemical measurements were operated on a CHI 760E electrochemical workstation (Chenhua, Shanghai, China), where a typical three-electrode system was carried out by using a bare or modified gold electrode (Au, 0.5 mm in diameter, working electrode), a platinum wire (counter electrode), and a saturated calomel electrode (SCE, reference electrode). The morphology or chemical constitution of AuPd@GO composite was monitored with a high-resolution transmission electron microscope (JEM-2100F, HR-TEM), which always accompanied by an energy-dispersive X-ray spectrometer (EDS, Oxford-1NCA) under an acceleration voltage of 200 kV. X-ray diffraction measurements (XRD) were managed by a Philips PW3040/60 diffractometer system involving Cu Kα radiation ($\lambda = 0.15405$ nm). The Research Quartz Crystal Microbalance (RQCM) system (MaxTek Inc., USA) was used to monitor the resonant frequency changes of a quartz crystal resonator.

Preparation of Ab_{Ac}-AuPd@GO

The preparation process of AuPd@GO composite was as follows: firstly, 1.77 g of $PdCl_2$ was dissolved into 0.4 mL of HCl solution (37%), then diluted to 100 mL with twice-distilled water to obtain H_2PdCl_4 stock solution (100 mM). $HAuCl_4$ solution (100 mM) was also obtained by using twice-distilled water and acted as stock solution. Next, GO was dispersed by ultrasonication for 30 min to prepare 1 mg mL^{-1} GO

dispersion. After that, the two stock solutions above were added together to GO dispersion. Then, the mixture was stirred slowly for 30 min under continuous magnetism and exposed under Xe arc lamp irradiation for 30 min, later vacuum-dried at 60 °C for 24 h. Further, the obtained product (AuPd@GO) was hold under hydrogen flow in a tube furnace at 300 °C for 2 h. Finally, 10 μL of the above AuPd@GO solution was taken and Ab_{Ac} (5 μL, 10^{-3} mg L^{-1}, irradiated by laser for 30 s before use) was added, thus incubating at 37 °C for 4 h. Similarly, unmixed AuPd nanoparticles (AuPd, namely without GO) were also prepared for the contrast in our work.

Fabrication of the biosensor

Au: prior to modification The bare Au electrode was polished orderly with 1.0 and 0.3 μm Al_2O_3 powder, then rinsed with twice-distilled water, ethanol, and twice-distilled water successively under ultrasonication for 5 min. Finally, the neat Au electrode was dried under N_2 atmosphere.

$Peptide_{Ac}$/Au The clean Au electrode was dropped with 10 μL of substrate peptide solution (200 μM), then worked overnight at 4 °C and washed with the cleaning phosphate buffer. After it, the peptide-immobilized electrode was incubated by 1 mM mercaptoethanol (MCH) for 30 min to remove nonspecific adsorbed peptide. Next, the electrode was immersed into enzyme mixture (200 μL) containing HAT p300 with various concentrations, Ac-CoA (500 μM), and HAT reaction buffer at 30 °C for 80 min. With regard to inhibitor test, C646 with different concentrations was introduced into the enzyme mixture above under the same condition. Again, the concentration of HAT p300 was 100 nM except concentration gradient experiment.

Ab_{Ac}-AuPd@GO/$peptide_{Ac}$/Au Ultimately, 10 μL of Ab_{Ac}-AuPd@GO was coated into the $peptide_{Ac}$/Au electrode surface for 30 min at 37 °C, then washed with the cleaning phosphate buffer. These electrodes were put in a 4 °C refrigerator when not in use.

Results and discussion

Design strategy

The electrochemical mechanism of our constructed AuPd@GO-based immunosensor for sensitive detection of HAT is depicted in Scheme 1. To begin with, the substrate peptide is immobilized on the Au surface by Au-S interaction. In the following HAT p300–derived acetylation process, the mixture of Ac-CoA and target p300 with different concentrations is added to the peptide-based electrode. As long as target p300 exists, lysine residues of substrate peptides which stand at the electrode surface could be acetylated, thus endowing with the capacity to couple with Ab_{Ac}. Based on it, in this way, we can introduce the AuPd@GO nanomaterial as a signal unit due to the response to TMB solution. Actually, GO, which is a one-atom-thick two-dimensional sheet and involves a number of distinctive properties, such as high mechanical stiffness and thermal conductivity, extraordinary electronic transport properties, and high specific surface area, enables to promote the stability of nanocatalysts (this refers to AuPd). It is precisely because catalysis is a surface effect, and the larger the specific surface area, the better the catalytic performance. Consequently, the GO-supported AuPd nanomaterial can offer both a high surface area and a conductive surface. It goes without saying that the AuPd@GO nanomaterial is very beneficial to electron transfer in TMB-related catalytic processes. This rationalized design is the key to fabricate the immunosensor for quantitative analysis of HAT p300 successfully.

Feasibility study

The transmission electron microscopy (TEM) was carried out for the morphology of GO and AuPd@GO. As illustrated in Fig. 1a, GO shows a thin layer and a large specific surface area. Moreover, there are a large number of dispersive particles uniformly inserted onto the surfaces of GO (Fig. 1b). As presented in the inset of Fig. 1b, it is obvious that the particle size of AuPd attached to GO is approximately 25 nm. Additionally, the EDS spectrum reveals vividly the coexistence of Au, Pd, and C (Fig. 1c).

Further test for the AuPd@GO nanomaterial is performed by X-ray diffraction (XRD) analysis (Fig. 1d). The representative diffraction peaks are located approximately at 40°, 46°, 67°, and 80°, which correspond to the (111), (200), (220), and (311) planes of the face-centered cubic AuPd alloy, respectively [40]. Additionally, the evident diffraction peak approximately at 23° is oriented in the (002) plane of GO [40]. Also, the selective area electron diffraction (SAED) pattern is shown in the inset of Fig. 1d; some bright spots from inner to outer corresponding to the (111), (200), (220), and (311) planes of the AuPd alloy are observed clearly, further demonstrating the formation of the AuPd nanomaterial with the highly crystalline nature [41].

Electrochemical impedance spectroscopy (EIS) is frequently used for investigating the layer-by-layer modifications, in which $[Fe(CN)_6]^{3-/4-}$ redox couple serves as the electrochemical probe (Fig. 2a). As the substrate peptides are immobilized onto Au surface (the figure is not shown), the charge transfer resistance (R_{ct}) drastically increases compared with that of bare Au due to the blocking effects of peptide on electron transfer. Next, R_{ct} at $peptide_{Ac}$/Au shows a consecutive increase as the acetylation reaction occurs. But, with the

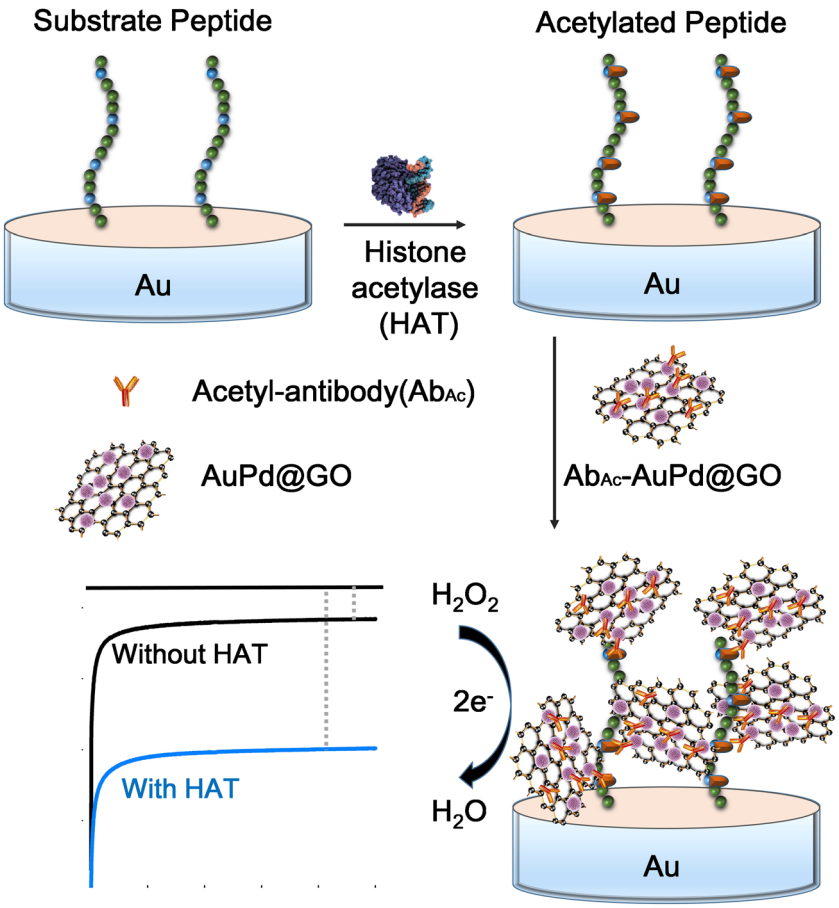

Scheme 1 The schematic representation of the electrochemical biosensor for probing the activity of HAT based on the AuPd@GO nanomaterial

successful combination of Ab_{Ac}-AuPd@GO, R_{ct} of the final electrode dramatically reduces. These results imply not only the special acetyl-Ab_{Ac} interaction but also the AuPd@GO-accelerated interfacial electron transfers.

To construct the similar biosensing interface, the substrate peptides are assembled on the surface of the specific QCM Au chip through Au-S bond. The gradual change of frequency is observed notably at $peptide_{Ac}$/Au in contrast to the bare Au chip, and the downward tendency illustrates the effective immobilization of the peptide on the surface of the chip (Fig. 2b). Furthermore, the frequency shift is dramatically enhanced after the interaction between Ab_{Ac}-AuPd@GO and acetyl of the acetylation peptide. The QCM results are consistent with that of EIS, confirming the successful preparation of the proposed biosensor.

Amperometric *i-t* curve provides an effective technique for characterizing the nanocatalyst-based electrochemical process. A decay curve for current and time relationship is displayed with a fixed potential of 150 mV after the appearance of a plateau (steady-state current) within 100 s. There is barely change on electrochemical signal at $peptide_{Ac}$/Au relative to bare Au, but the visible difference of the electrochemical signal apparently at Ab_{Ac}-AuPd@GO/$peptide_{Ac}$/Au appears due to the occurrence of electrocatalysis (Fig. 2c). The main reason is that TMB, which can diffuse into and out of the redox site of the AuPd@GO, acts as an electron shuttle and simultaneously couples the catalytic reduction of H_2O_2, leading to the remarkable electrocatalytic current. In addition, as shown in Fig. S1 (see ESM), insignificant electrochemical signal appears at GO-based electrode; on the contrary, there is an outstanding signal at AuPd@GO-based electrode. Still, a weaker electrocatalytic performance can also be observed at the AuPd-based electrode, and the interesting phenomenon can be attributive to the missing GO with highly loading and supporting capacity. At the same time, a similar tendency takes place at the two different concentrations of HAT p300. These results prove that the AuPd@GO is a well-pleasing catalyst in our work.

We also find that if the substrate peptide is acetylated by HAT p300 together with the co-substrate Ac-CoA, an evident electrochemical signal amplification will occur, indicating that the acetylation reaction proceeds smoothly. As shown in Fig. 2d, the amperometric current for 100 nM of p300 is over 10 times larger than that in the absence of p300. Simultaneously, a reaction solution with missing components including HAT p300, peptide, or Ac-CoA coated the electrode surface, and the negligible electrochemical signal is presented (ESM Fig. S2A). We

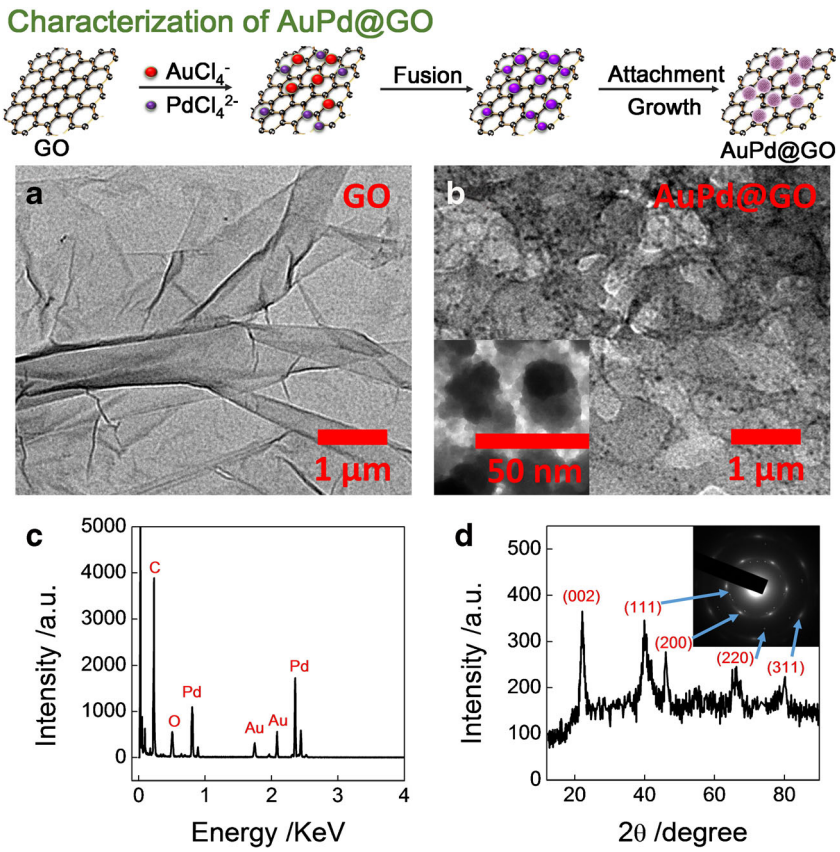

Fig. 1 TEM images of **a** GO and **b** AuPd@GO (inset: enlarged view). **c** EDS spectrum and **d** XRD patterns of AuPd@GO (inset: SAED pattern)

further carry out an in-depth study of both the electrocatalytic ability of the AuPd@GO nanomaterial and the acetylation of HAT p300. As illustrated in Fig. S2B (see ESM), the acetylation reaction–caused or its CPY-treated product is examined, and whether there is CPY or not, there is still a strong signal. This suggests that the acetylated peptide can prevent the CPY-degradation effect, which takes on a protective role. These results illustrate indirectly the acetylation process is in line with our expectation.

Probing activity of HAT p300

To acquire the best electrochemical performance of the favorable platform, some experiment conditions involving time or temperature of acetylation, and incubation time or temperature of antigen-antibody interaction are discussed. As depicted in Fig. S3A (see ESM), the electrochemical current increases gradually from 0 to 80 min and reaches the maximum value at 80 min. So, the optimal acetylation time is determined to be 80 min. At the moment, the electrochemical current increases with the acetylation temperature from 0 to 30 °C as well and then begins to reduce after 30 °C (ESM Fig. S3B). Hence, 30 °C is considered he optimal acetylation time. In a similar way, 30 min and 37 °C are chosen as the optimal combination time and temperature, respectively (ESM Fig. S3C and D).

Under the optimal experimental conditions, the amperometric *i-t* curves of AuPd@GO-based electrode for HAT p300 with various concentrations are detected to evaluate the sensitivity of the proposed method. As shown in Fig. 3a, with the increase of HAT p300 concentration in the range from 1 pM to 1000 nM, the *i-t* responses increase gradually. Moreover, it also exhibits a good linear relationship with the logarithm of HAT p300 (Fig. 3b). The relevant calibration curve of the proposed biosensor for quantitative HAT p300 analysis could be obtained with a detection limit of 0.5 pM ($S/N = 3$). Additionally, the lower detection limit is displayed by comparing with other HAT p300 biosensors which are showed in Table S1 (see ESM). Further, the concentration effect of HAT p300 at the AuPd-based electrode is also investigated to reflect the outstanding performance of AuPd@GO. As depicted in Fig. 3b, there is a sharply difference on the electrochemical signal between AuPd-based and AuPd@GO-based electrodes, and the latter has a better electrocatalytic performance. It is noticeable that the outstanding electrochemical signal depends on not only AuPd nanoparticles with electrocatalytic properties but also GO with splendid load capacity.

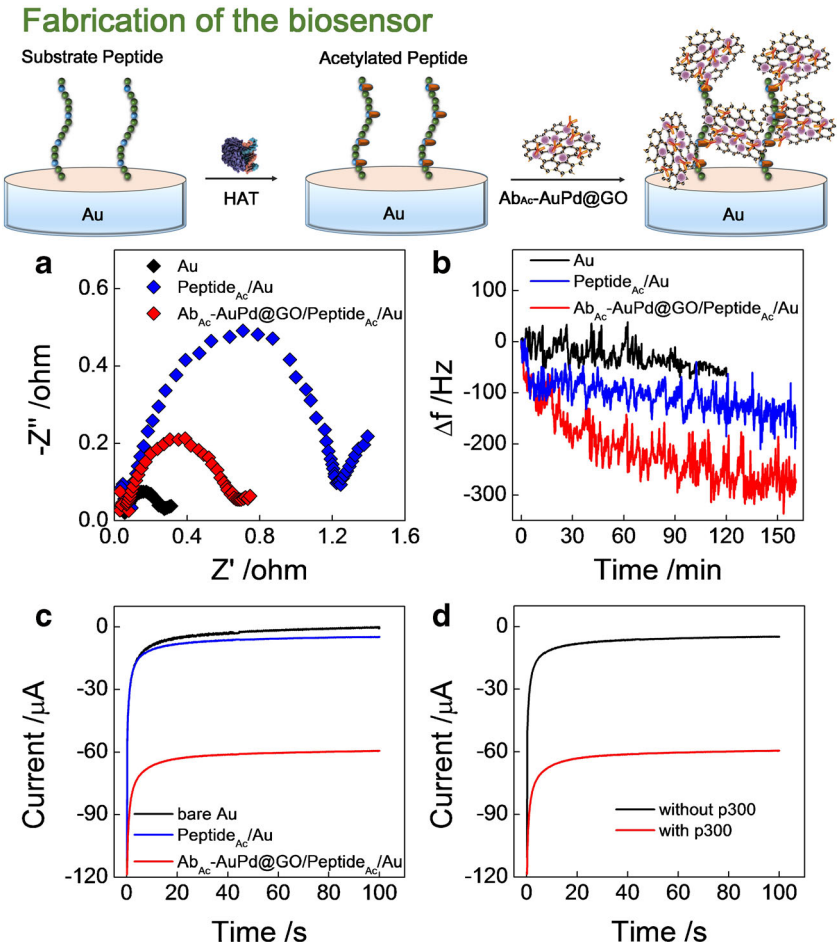

Fig. 2 **a** EIS of the modified electrodes with the frequency of 10^5 to 10^{-2} Hz at an amplitude of 5 mV in 5 mM $[Fe(CN)_6]^{3-/4-}$ containing 0.1 M KCl. **b** QCM of the modified electrodes in PBS; amperometric *i-t* curves (current versus time) at 150 mV in PBS containing TMB solution of **c** the modified electrodes and **d** the electrodes before or after acetylation

To investigate the role of HAT p300 inhibitor, AuPd@GO-based electrode is employed by probing different amounts of the inhibitor. In this case, C646, as a potent HAT inhibitor, is selected to explore inhibitors screening with respect to the acetylation. As can be seen from Fig. 3c, the electrochemical signal is reduced with the introduction of C646. Figure 3d also depicts that the electrochemical signal at AuPd@GO-based electrode decreases gradually with the increasing concentration of C646, demonstrating an obvious inhibiting effect. Despite the same trend, the electrochemical signal at AuPd-based electrode is much smaller than that of our proposed biosensor, proving the superiority of the AuPd@GO nanomaterial. IC_{50} value is the concentration of the inhibitor leading to the half-maximal inhibition of the enzyme activity, which is calculated to be 28.9 μM in our work. Hence, this proposed sensor holds tremendous promise in the small-molecule inhibitor analysis.

The practical application of the biosensor

In order to investigate the specificity, the biosensor is used for testing the four interfering proteins, such as PKA, AChE, TdT, and ALP. As shown in Fig. 4a, relatively low signals of the four enzymes are observed compared with HAT p300. Additionally, when the biosensor is applied for the mixture containing HAT p300 and the one of the four enzymes, the current is almost the same as that of HAT p300 only, indicating good specificity and nice anti-interference for HAT p300 detection. Furthermore, to evaluate the clinical practicability, the influences of some routine interfering substances at very high concentrations which are mentioned in the Clinical and Laboratory Standards Institute (CLSI) guidelines are also studied. As shown in Fig. S4A (see ESM), the biosensor displays a high selectivity for HAT p300, which is attributed to the occurrence of acetylation. Not only that, the current signal does not change significantly with the addition of these interfering substances to acetylation solution (ESM Fig. S4B). These results indicate that such a detection system exhibits remarkably high anti-interference.

To test the persistent electrocatalytic effect, a current-time stage curve on successive H_2O_2 and ascorbic acid (AA) interval additions is exposed in Fig. 4b with the time range from 0 to 1800 s. It is realized that the steady-state signals reach a

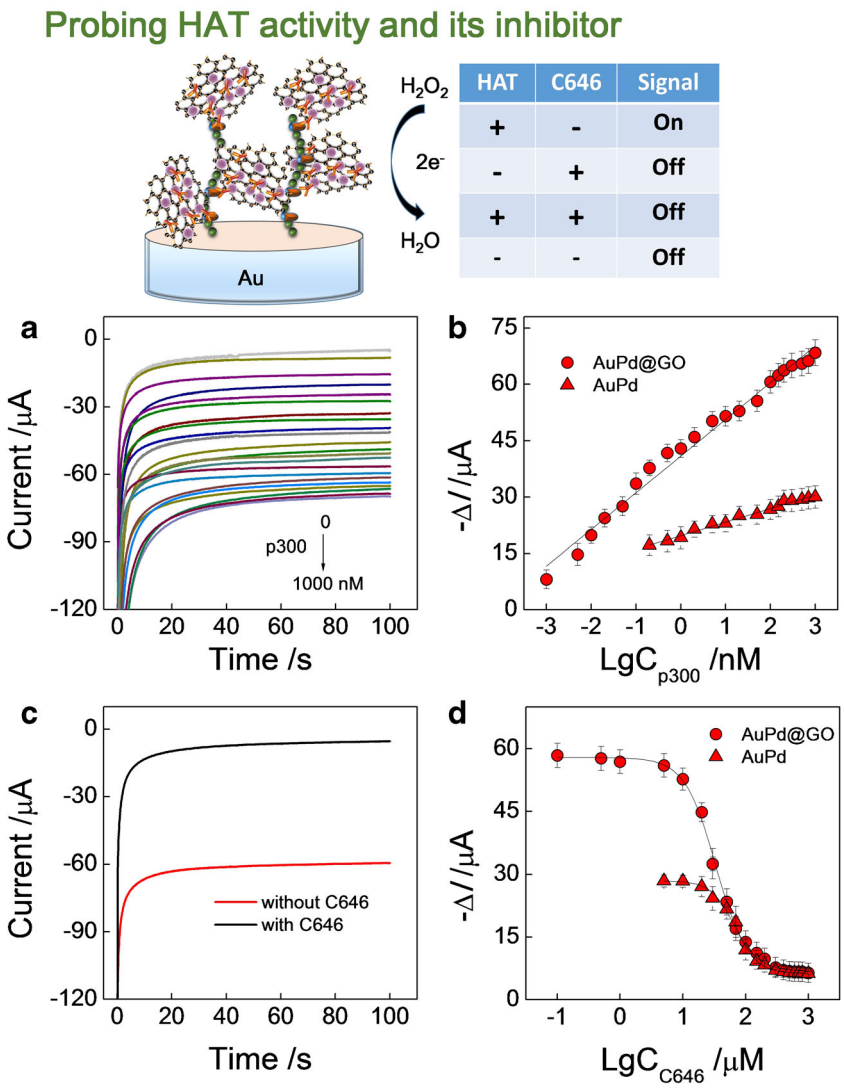

Fig. 3 **a** Amperometric *i-t* curves at 150 mV of the biosensor in PBS containing TMB solution correspond to different concentrations of HAT p300 from top to bottom: 0, 0.001, 0.005, 0.01, 0.02, 0.05, 0.1, 0.2, 0.5, 1, 2, 5, 10, 20, 50, 100, 150, 200, 300, 500, 700, and 1000 nM. **b** The linear calibration curve of current response with logarithm of HAT p300 concentrations at AuPd@GO- or AuPd-based electrodes. **c** Amperometric *i-t* curves at 150 mV in PBS containing TMB solution in the presence or absence of C646. **d** Electrochemical signal as a function of the concentrations of C646 (0, 0.1, 0.5, 1.0, 5.0, 10, 20, 30, 50, 70, 100, 150, 200, 300, 400, 500, 600, 700, 800, and 1000 μM) at AuPd@GO- or AuPd-based electrodes

stable value in less than 2 s, showing a fast amperometric response performance. As expected, the sensors under different HAT p300 concentrations involving 1 nM and 100 nM respond sensitively to each addition for H_2O_2, yielding steady-state signals. However, with the introduction of AA alternately, there is negligible change in the electrochemical current. Even importantly, when greater than 1800 s, the catalytic effect is consistent. These results illustrate the AuPd@GO-based electrochemical biosensor can give a sensitive and rapid response to H_2O_2 successfully. Nay, the differential signal change at 1 nM and 100 nM HAT p300 suggests further the feasibility of the strategy for HAT p300 detection again.

The long-term storage stability of the AuPd@GO-based biosensor is investigated by measuring every 5 days over a period of 30 days and judged via storing it at 4 °C refrigerator (Fig. 4c). It is found that about 92.7% of initial current keeps after 15 days. And then, the value maintains about 86.5% of the initial value after 30 days. The results illustrate a satisfactory stability of the prepared biosensor. By preforming the same HAT concentration (1 nM and 100 nM, respectively) on the eight prepared electrodes under the same condition, the reproducibility of the biosensor can be explored in Fig. 4d. The relative standard deviation (RSD) of the biosensor is 3.7% ($n = 4$), which reveals acceptable reproducibility for the strategy.

Real sample analysis

Recovery experiments are performed by evaluating the applicability and reliability of the immunosensor for the HAT p300 analysis. Briefly, the real samples are spiked with different concentrations of HAT p300 into 10-fold-diluted cell lysates, blood and urine samples (obtained from Hunan Provincial People's Hospital, China). The experimental results are showed in Table S2 (see ESM). From ESM Table S2, the recoveries vary from 97.4 to 103% in cell lysates, 97.8% to 102% in blood, and

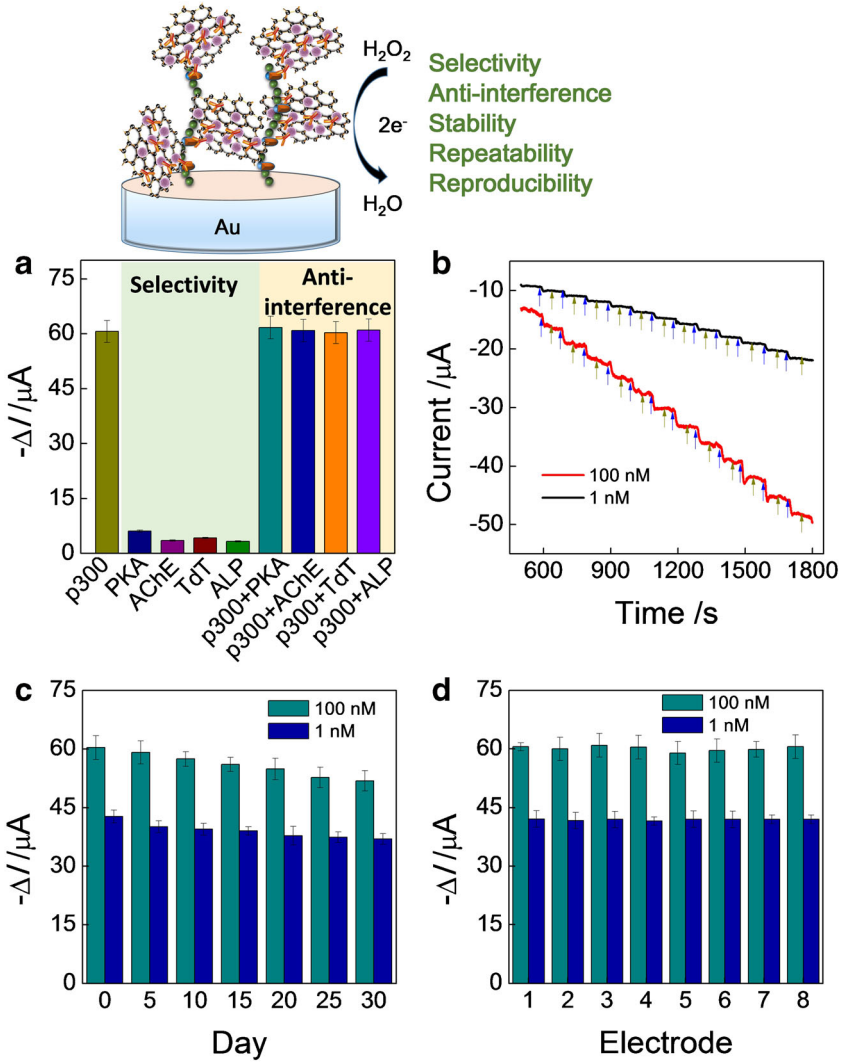

Fig. 4 **a** The selectivity and anti-interference test of the assay in PBS containing TMB solution for HAT p300. **b** Typical current-time response curves for the addition of H_2O_2 (blue arrow) and ascorbic acid (AA, brown arrow) alternately in PBS. **c** Stability and **d** reproducibility tests of the biosensor in PBS containing TMB solution at 1-nM and 100-nM target, respectively

99.2% to 101.5% in urine, respectively. These satisfying RSDs indicate that the developed immunosensor possesses a well application prospect in clinical research as well.

Conclusions

In summary, we design a novel electrochemical immunosensor by using AuPd@GO composite as both identification probe and signal probe. The immunosensor is used for the HAT p300 analysis by the typical *i-t* technique with the unique features such as the high sensitivity and fast response. Because the AuPd@GO composite takes advantages of the remarkable electrocatalytic activity, the good conductivity, and high surface area, the AuPd@GO-derived electrocatalytic signal is amplified greatly, resulting in nice analytical performance. Compared with other protocols, wide linear range and low detection limit are obtained. Even more importantly, this immunosensor can be applied favorably for rapid and sensitive detection of the HAT p300–related inhibitor. The proposed method provides a promising alternative for constructing HAT p300–based immunosensor.

Funding information This work received financial support from the National Natural Science Foundation of China (21605089 and 81773483), the Ningbo Municipal Natural Science Foundation (2017A610231 and 2018A610217), the Open Subject of State Key Laboratory of Chemo/Biosensing and Chemometrics (2016001), and Zhejiang Provincial Natural Science Foundation of China (LGF18B070002). This work was also sponsored by K.C. Wong Magna Fund in Ningbo University.

Compliance with ethical standards This study was approved by the Regional Ethics Committee of the Hunan Provincial People's Hospital, and the blood and urine samples from the Hunan Provincial People's Hospital in this study are permitted by patients through signed informed consents.

Conflict of interest The authors declare that they have no competing interests.

References

1. Doll S, Burlingame AL. Mass spectrometry-based detection and assignment of protein posttranslational modifications. ACS Chem Biol. 2015;10(1):63–71.
2. Casey AK, Orth K. Enzymes involved in AMPylation and deAMPylation. Chem Rev. 2018;118(3):1199–215.
3. Li C, Wang LX. Chemoenzymatic methods for the synthesis of glycoproteins. Chem Rev. 2018;118(17):8359–413.
4. Klein T, Eckhard U, Dufour A, Solis N, Overall CM. Proteolytic cleavage-mechanisms, function, and "Omic" approaches for a near-ubiquitous posttranslational modification. Chem Rev. 2018;118(3):1137–68.
5. Ali I, Conrad RJ, Verdin E, Ott M. Lysine acetylation goes global: from epigenetics to metabolism and therapeutics. Chem Rev. 2018;118(3):1216–52.
6. Kang K, Choi JM, Fox JM, Snyder PW, Moustakas DT, Whitesides GM. Acetylation of surface lysine groups of a protein alters the organization and composition of its crystal contacts. J Phys Chem B. 2016;120(27):6461–8.
7. McCullough CE, Marmorstein R. Molecular basis for histone acetyltransferase regulation by binding partners, associated domains, and autoacetylation. ACS Chem Biol. 2016;11(3):632–42.
8. Zou Y, Zhang HX, Wang ZH, Liu QY, Liu Y. A novel ECL method for histone acetyltransferases (HATs) activity analysis by integrating HCR signal amplification and ECL silver clusters. Talanta. 2019;198:39–44.
9. Michaelides MR, Kluge A, Patane M, Van Drie JH, Wang C, Hansen TM, et al. Discovery of spiro oxazolidinediones as selective, orally bioavailable inhibitors of p300/CBP histone acetyltransferases. ACS Med Chem Lett. 2018;9(1):28–33.
10. Han Z, Chou CW, Yang XK, Bartlett MG, Zheng YG. Profiling cellular substrates of lysine acetyltransferases GCN5 and p300 with orthogonal labeling and click chemistry. ACS Chem Biol. 2017;12(6):1547–55.
11. Green KD, Biswas T, Pang AH, Willby MJ, Reed MS, Stuchlik O, et al. Acetylation by eis and deacetylation by Rv1151c of mycobacterium tuberculosis HupB: biochemical and structural insight. Biochemistry. 2018;57(5):781–90.
12. Young IA, Mittal C, Shogren-Knaak MA. Expression and purification of histone H3 proteins containing multiple sites of lysine acetylation using nonsense suppression. Protein Expr Purif. 2016;118:92–7.
13. Bonhoure A, Vallentin A, Martin M, Senff-Ribeiro A, Amson R, Telerman A, et al. Acetylation of translationally controlled tumor protein promotes its degradation through chaperone-mediated autophagy. Eur J Cell Biol. 2017;96(2):83–98.
14. Bose DA, Donahue G, Reinberg D, Shiekhattar R, Bonasio R, Berger SL. RNA binding to CBP stimulates histone acetylation and transcription. Cell. 2017;168(1–2):135–49.
15. Aljayyoussi G, Gumbleton M. A novel cost-effective approach for the efficient radiolabeling of dendritic macromolecules with a β-emitting radiotracer. Tetrahedron Lett. 2013;54(9):1045–8.
16. Thakkar A, Wavreille AS, Pei D. Traceless capping agent for peptide sequencing by partial edman degradation and mass spectrometry. Anal Chem. 2006;78(16):5935–9.
17. Baral A, Asokan A, Bauer V, Kieffer B, Torbeev V. Chemical synthesis of transactivation domain (TAD) of tumor suppressor protein p53 by native chemical ligation of three peptide segments. Tetrahedron. 2019;75(6):703–8.
18. Park H, You S, Kim J, Kim W, Do J, Jang Y, et al. Seventeen O-acetylated N-glycans and six O-acetylation sites of Myozyme identified using liquid chromatography-tandem mass spectrometry. J Pharm Biomed. 2019;169:188–95.
19. Felix FS, Angnes L. Electrochemical immunosensors-a powerful tool for analytical applications. Biosens Bioelectron. 2018;102:470–8.
20. Wen W, Yan X, Zhu CZ, Du D, Lin YH. Recent advances in electrochemical immunosensors. Anal Chem. 2017;89(1):138–56.
21. Liu YB, Xu LP, Wang SQ, Yang WZ, Wen YQ, Zhang XJ. An ultrasensitive electrochemical immunosensor for apolipoprotein E4 based on fractal nanostructures and enzyme amplification. Biosens Bioelectron. 2015;71:396–400.
22. Yu ZZ, Tang Y, Cai GN, Ren RR, Tang DP. Paper electrode-based flexible pressure sensor for point-of-care immunoassay with digital multimeter. Anal Chem. 2019;91:1222–6.
23. Zeng RJ, Luo ZB, Zhang LJ, Tang DP. Platinum nanozyme-catalyzed gas generation for pressure-based bioassay using polyaniline nanowires-functionalized graphene oxide framework. Anal Chem. 2018;90:12299–306.
24. Pang PF, Teng X, Chen M, Zhang YL, Wang HB, Yang C, et al. Ultrasensitive enzyme-free electrochemical immunosensor for microcystin-LR using molybdenum disulfide/gold nanoclusters nanocomposites as platform and Au@Pt core-shell nanoparticles as signal enhancer. Sensors Actuators B Chem. 2018;266:400–7.
25. Tang QR, Zhang LH, Tan XF, Jiao L, Wei Q, Li H. Bioinspired synthesis of organic-inorganic hybrid nanoflowers for robust enzyme-free electrochemical immunoassay. Biosens Bioelectron. 2019;133:94–9.
26. Fu Y, Xu P, Huang D, Zeng G, Lai C, Qin L, et al. Au nanoparticles decorated on activated coke via a facile preparation for efficient catalytic reduction of nitrophenols and azo dyes. Appl Surf Sci. 2019;473:578–88.
27. Zhang Z, Shi H, Wu Q, Bu X, Yang Y, Zhang J. Hierarchical structure based on Au nanoparticles and porous CeO_2 nanorods: enhanced activity for catalytic applications. Mater Lett. 2019;242:20–3.
28. Zeng RJ, Luo ZB, Su LS, Zhang LJ, Tang DP, Niessner R, et al. Palindromic molecular beacon based Z-scheme BiOCl-Au-CdS photoelectrochemical biodetection. Anal Chem. 2019;91:2447–54.
29. Mandal R, Baranwal A, Srivastava A, Chandra P. Evolving trends in bio/chemical sensor fabrication incorporating bimetallic nanoparticles. Biosens Bioelectron. 2018;117:546–61.
30. Chen X, Shen Y, Zhou P, Zhong X, Li G, Han C, et al. Bimetallic Au/Pd nanoparticles decorated ZnO nanowires for NO_2 detection. Sensors Actuators B Chem. 2019;289:160–8.
31. Xia H, An J, Hong M, Xu S, Zhang L, Zuo S. Aerobic oxidation of 5-hydroxymethylfurfural to 2,5-difurancarboxylic acid over Pd-Au nanoparticles supported on Mg-Al hydrotalcite. Catal Today. 2019;319:113–20.
32. Zhang Y, Gao F, Fu ML. Composite of Au-Pd nanoalloys/reduced graphene oxide toward catalytic selective organic transformation to fine chemicals. Chem Phys Lett. 2018;691:61–7.
33. Hatamluyi B, Lorestani F, Es'haghi Z. Au/Pd@rGO nanocomposite decorated with poly (L-cysteine) as a probe for simultaneous sensitive electrochemical determination of anticancer drugs, ifosfamide and etoposide. Biosens Bioelectron. 2018;120:22–9.
34. Raghavendra P, Reddy GV, Sivasubramanian R, Chandana PS, Sarma LS. Reduced graphene oxide-supported Pd@Au bimetallic nano electrocatalyst for enhanced oxygen reduction reaction in alkaline media. Int J Hydrog Energy. 2018;43(8):4125–35.
35. Cai GN, Yu ZZ, Ren RR, Tang DP. Exciton-plasmon interaction between AuNPs/graphene nanohybrids and CdS quantum dots/TiO_2 for photoelectrochemical aptasensing of prostate-specific antigen. ACS Sens. 2018;3:632–9.
36. Tahriri M, Monico MD, Moghanian A, Yaraki MT, Torres R. Yadegari, graphene and its derivatives: opportunities and challenges in dentistry. Mater Sci Eng C Mater. 2019;102:171–85.

37. Wang J, Jin X, Li C, Wang W, Wu H, Guo S. Graphene and graphene derivatives toughening polymers: toward high toughness and strength. Chem Eng J. 2019;370:831–54.
38. Vashist SK, Luppa PB, Yeo LY, Ozcan A, Luong JHT. Emerging technologies for next-generation point-of-care testing. Trends Biotechnol. 2015;33:692–705.
39. Hu YF, Chen SY, Han YT, Chen HJ, Wang Q, Nie Z, et al. Unique electrocatalytic activity of a nucleic acid-mimicking coordination polymer for the sensitive detection of coenzyme A and histone acetyltransferase activity. Chem Commun. 2015;51:17611–4.
40. Yang HM, Zhang Y, Li L, Sun GQ, Zhang LN, Ge SG, et al. Real-time and in situ enzyme inhibition assay for the flux of hydrogen sulfide based on 3D interwoven AuPd-reduced graphene oxide network. Biosens Bioelectron. 2017;87:53–8.
41. Li J, Tang W, Huang J, Jin J, Ma J. Polyethyleneimine decorated graphene oxide-supported $Ni_{1-x}Fe_x$ bimetallic nanoparticles as efficient and robust electrocatalysts for hydrazine fuel cells. Catal Sci Technol. 2013;3:3155–62.